A&A 455, 879–890 (2006)
DOI: 10.1051/0004-6361:20053645

Astronomy & Astrophysics

The VIMOS VLT Deep Survey⋆

Evolution of the luminosity functions by galaxy type up to z = 1.5 from first epoch data

E. Zucca[1], O. Ilbert[2,3], S. Bardelli[1], L. Tresse[3], G. Zamorani[1], S. Arnouts[3], L. Pozzetti[1], M. Bolzonella[2], H. J. McCracken[10,11], D. Bottini[4], B. Garilli[4], V. Le Brun[3], O. Le Fèvre[3], D. Maccagni[4], J. P. Picat[5], R. Scaramella[6], M. Scodeggio[4], G. Vettolani[6], A. Zanichelli[6], C. Adami[3], M. Arnaboldi[7], A. Cappi[1], S. Charlot[8,10], P. Ciliegi[1], T. Contini[5], S. Foucaud[4], P. Franzetti[4], I. Gavignaud[5,12], L. Guzzo[9], A. Iovino[9], B. Marano[2], C. Marinoni[9], A. Mazure[3], B. Meneux[3], R. Merighi[1], S. Paltani[3], R. Pellò[5], A. Pollo[9], M. Radovich[7], M. Bondi[6], A. Bongiorno[2], G. Busarello[7], O. Cucciati[9], L. Gregorini[6], F. Lamareille[5], G. Mathez[5], Y. Mellier[10,11], P. Merluzzi[7], V. Ripepi[7], and D. Rizzo[5]

[1] INAF – Osservatorio Astronomico di Bologna, via Ranzani 1, 40127 Bologna, Italy
e-mail:elena.zucca@oabo.inaf.it
[2] Università di Bologna, Dipartimento di Astronomia, via Ranzani 1, 40127 Bologna, Italy
[3] Laboratoire d'Astrophysique de Marseille (UMR 6110), CNRS-Université de Provence, BP 8, 13376 Marseille Cedex 12, France
[4] INAF – IASF, via Bassini 15, 20133 Milano, Italy
[5] Laboratoire d'Astrophysique de l'Observatoire Midi-Pyrénées (UMR 5572), 14 avenue E. Belin, 31400 Toulouse, France
[6] INAF – IRA, via Gobetti 101, 40129 Bologna, Italy
[7] INAF – Osservatorio Astronomico di Capodimonte, via Moiariello 16, 80131 Napoli, Italy
[8] Max Planck Institut fur Astrophysik, 85741 Garching bei München, Germany
[9] INAF – Osservatorio Astronomico di Brera, via Brera 28, 20121 Milano, Italy
[10] Institut d'Astrophysique de Paris (UMR 7095), 98 bis Bvd Arago, 75014 Paris, France
[11] Observatoire de Paris, LERMA, 61 Avenue de l'Observatoire, 75014 Paris, France
[12] European Southern Observatory, Karl-Schwarzschild-Strasse 2, 85748 Garching bei München, Germany

Received 16 June 2005 / Accepted 2 May 2006

ABSTRACT

From first epoch observations of the VIMOS VLT Deep Survey (VVDS) we have derived luminosity functions for galaxy samples selected by spectral type out to $z = 1.5$. With the VVDS we are able to investigate *within the same sample* the evolution of the type dependent luminosity function selected in several rest-frame bands over 70% of the age of the Universe. The simple $I_{\rm AB} = 24$ VVDS magnitude limit is significantly fainter than other complete spectroscopic surveys and allows the determination of the faint end slope of the luminosity function with unprecedented accuracy. Galaxies have been classified in four spectral types, from early type to irregular galaxies, using their colours and redshift. Luminosity functions have been computed in the U, B, V, R and I rest frame bands for each type, in redshift bins from $z = 0.05$ to $z = 1.5$. In all the considered rest frame bands, we find a significant steepening of the luminosity function from early to late types. The characteristic luminosity M^* of the Schechter function is significantly fainter for late type galaxies and this difference between types increases in the redder bands. For each spectral type we find a brightening of M^* with increasing redshift, ranging from $\lesssim$0.5 mag for early type galaxies to ∼1 mag for the latest type galaxies, while the slope of the luminosity function of each spectral type is consistent with being redshift-independent. The luminosity function of early type galaxies is consistent with passive evolution up to $z \sim 1.1$, whilst the number of bright ($M_{B_{\rm AB}} < -20$) early type galaxies has decreased by ∼40% from $z \sim 0.3$ to $z \sim 1.1$. The normalisation of the luminosity function of latest type galaxies evolves strongly with redshift with an increase of more than a factor 2 from $z \sim 0.3$ to $z \sim 1.3$: the density of bright ($M_{B_{\rm AB}} < -20$) late type galaxies in the same redshift range increases of a factor ∼6.6. These results indicate a strong type-dependent evolution and identifies the latest spectral types as responsible for most of the evolution of the UV-optical luminosity function out to $z = 1.5$.

Key words. galaxies: evolution – galaxies: luminosity function, mass function – galaxies: statistics – surveys

1. Introduction

An unbiased and detailed characterization of the luminosity function (LF) of field galaxies is a basic requirement in many extragalactic studies.

At present the local luminosity function is well determined by the results obtained by the 2dF Galaxy Redshift Survey (2dFGRS, Norberg et al. 2002) and by the Sloan Digital Sky Survey (SDSS, Blanton et al. 2003). These surveys measure redshifts for 10^5–10^6 galaxies over a large area, and therefore explore well the properties of the local ($z < 0.3$) Universe. Large samples such as these also allows one to study the luminosity functions (as well as the correlation functions and other properties) for galaxies of different types, defined on the basis of colours and/or spectral properties. A critical analysis of the

⋆ Based on data obtained with the European Southern Observatory Very Large Telescope, Paranal, Chile, program 070.A-9007(A), and on data obtained at the Canada-France-Hawaii Telescope, operated by the CNRS of France, CNRC in Canada and the University of Hawaii.

luminosity functions depending on galaxy type as measured from the various redshift surveys, as well as a comparison of the different results, can be found in de Lapparent (2003).

Madgwick et al. (2002), analyzing 2dFGRS data, find a systematic steepening of the faint end slope and a faintening of M^* of the luminosity function as one moves from passive to active star forming galaxies. Similar results are found by Blanton et al. (2001) for the SDSS sample, moving from the redder to the bluer galaxies.

In the high redshift Universe, several studies over the past decade have attempted to map the evolution of the luminosity function. However, because of the long integration times required to obtain spectra of high redshift galaxies, spectroscopic surveys were limited only a few hundred objects. For example, the Canadian Network for Observational Cosmology field galaxy redshift survey (CNOC-2, Lin et al. 1999) and the ESO Sculptor Survey (ESS, de Lapparent et al. 2003) derived the luminosity function up to $z \sim 0.5$ using ∼2000 and ∼600 redshifts, respectively. de Lapparent et al. (2003) find a behaviour of the LF by type similar to the local one derived from 2dFGRS and a strong evolution of a factor two in the volume density of the late type galaxies with respect to the early type galaxies. Lin et al. (1999) find for early type galaxies a positive luminosity evolution with increasing redshift, which is almost compensated by a negative density evolution. On the contrary, for late type galaxies they find a strong positive density evolution, with nearly no luminosity evolution. At higher redshift, the Canada France Redshift Survey (CFRS, Lilly et al. 1995) studied the galaxy luminosity function up to $z \sim 1.1$ with a sample of ∼600 redshifts. From this survey, the LF of the red population changes little with redshift, while the LF of the blue population brightens by about one magnitude from $z \sim 0.5$ to $z \sim 0.75$. Other results suggest a strong number density evolution of early type galaxies (Bell et al. 2004; Faber et al. 2006); conversely, in the K20 survey (Cimatti et al. 2002), Pozzetti et al. (2003) found that red and early type galaxies dominate the bright end of the LF and that their number density shows at most a small decrease (<30%) up to $z \sim 1$ (see also Saracco et al. 2006 and Caputi et al. 2006).

Luminosity function estimates at higher redshift or with larger samples have up to now been computed only using photometric redshifts, for example the COMBO-17 survey (Wolf et al. 2003) and the FORS Deep Field (FDF, Gabasch et al. 2004) and the Hubble Deep Fields (HDF-N and HDF-S, see e.g. Sawicki et al. 1997; Poli et al. 2001, 2003); most of these projects derived also the luminosity function for different galaxy types. Wolf et al. (2003) found that early type galaxies show a decrease of a factor ∼10 in ϕ^* up to $z = 1.2$. Latest type galaxies show a brightening of about one magnitude in M^* and a ϕ^* increase of a factor ∼1.6 in their highest redshift bin ($z \sim 1.1$) in the blue band. Giallongo et al. (2005), using HDFs data, find that the B band number densities of red and blue galaxies evolve differently, with a strong decrease of the red population at $z = 2$–3 and a corresponding increase of the blue population. Dahlen et al. (2005), using GOODS data, claim that the starburst population fraction increases with redshift by a factor of 3 at $z = 2$ in the U band.

Although photometric redshifts represent a powerful tool to investigate the distant Universe, their precision heavily depends on the quality of the input photometric data, the number of bands available, which templates are used and how the "training" procedure (with spectroscopic data) is performed; moreover, they are affected by the problem of "catastrophic errors", i.e. objects whose photometric redshift is completely different from the spectrocopic redshift. The VIMOS VLT Deep survey (VVDS, Le Fèvre et al. 2003b), together with the DEEP-2 Galaxy Redshift Survey (Davis et al. 2003), represent a significant advance. The VVDS is an ongoing program to map the evolution of galaxies, large-scale structures and AGNs from the redshift measurements of $\sim 10^5$ objects down to a magnitude $I_{\rm AB} = 24$, in combination with a multiwavelength dataset from radio to X-rays.

From an analysis of the evolution of the global luminosity function from the first epoch VVDS data (Ilbert et al. 2005), we found a significant brightening of the M^* parameter in the U, B, V, R and I rest frame bands, in the redshift interval $0.05 < z < 2$. Moreover, we measured an increase of the comoving density of bright galaxies: this increase depends on the rest frame bandpass, and is highest in the bluest bandpasses.

Among the other results of this survey, we recall the study of the radio selected objects (Bondi et al. 2003) and of their optical counterparts (Ciliegi et al. 2005), the evolution of the clustering properties (Le Fèvre et al. 2005b; Pollo et al. 2005) and of the bias parameter (Marinoni et al. 2005). Moreover, from the joint GALEX-VVDS sample, we determined the evolution of the far UV luminosity function (Arnouts et al. 2005) and luminosity density (Schiminovich et al. 2005).

In this paper we study the evolution of the luminosity functions of galaxies selected by spectral types based on the VVDS data. This sample allows to perform this analysis for the first time with excellent statistical accuracy over a large redshift range ($0.05 < z < 1.5$).

The plan of the paper is the following: in Sect. 2 we briefly present the first epoch VVDS sample, in Sect. 3 we describe the galaxy classification and in Sect. 4 we illustrate the method used to estimate the luminosity functions. In Sect. 5 we compare the luminosity functions of the different galaxy types and in Sect. 6 we show the evolution with redshift of the luminosity functions by type. Finally in Sect. 7 we compare our results with previous literature estimates and in Sect. 8 we summarise our results.

Throughout the paper we adopt a flat $\Omega_{\rm m} = 0.3$ and $\Omega_\Lambda = 0.7$ cosmology, with $h = H_0/100$ km s^{-1} Mpc^{-1}. Magnitudes are given in the AB system and are expressed in the five standard bands U (Bessel), B and V (Johnson), R and I (Cousins).

2. The first epoch VVDS sample

The VVDS is described in detail in Le Fèvre et al. (2005a): here we describe only the principle characteristics of the sample used for the analysis presented in this paper.

The entire VVDS comprises a "wide" component containing four unconnected fields (which is not used in this paper), and a "deep" part, with spectroscopy of objects selected with $17.5 \leq I_{\rm AB} \leq 24$ on the field 0226-04. Multicolour photometry is available for each field (Le Fèvre et al. 2004a): in particular, the B, V, R, I photometry for the 0226-04 deep field is described in detail in McCracken et al. (2003). Moreover, U band (Radovich et al. 2004) and J and K band (Iovino et al. 2005) data are available for smaller areas of these fields.

Starting from these photometric catalogues, spectroscopic observations were performed with the VIsible Multi–Object Spectrograph (VIMOS, Le Fèvre et al. 2003a) at the ESO Very Large Telescope (UT3). Objects were selected only by apparent magnitude, without any other colour or shape criteria.

In addition, deep spectroscopic observations ($17.5 \leq I_{\rm AB} \leq 24$) were carried out also on the Chandra Deep Field South (VVDS-CDFS, Le Fèvre et al. 2004b), based on the EIS I band photometry and astrometry (Arnouts et al. 2001). Multicolour U,

B, V, R and I photometry for this sample is available from the COMBO-17 survey (Wolf et al. 2003).

Spectroscopic data were reduced with the VIMOS Interactive Pipeline Graphical Interface (VIPGI, Scodeggio et al. 2005, Zanichelli et al. 2005) and redshift measurements were made using the "KBRED" package (Scaramella et al. 2006) and then visually checked. Each redshift measurement was assigned a quality flag, ranging from "0" (impossible to determine a redshift) to "4" (the measure is 100% certain); flag "9" indicates spectra with a single emission line, for which multiple solutions are possible. Further details on the quality flags are given in Le Fèvre et al. (2005a).

The analysis presented in this paper is based on the first epoch VVDS deep sample, obtained from autumn 2002 observations on the fields VVDS-02h and VVDS-CDFS, which covers 1750 and 450 arcmin^2, respectively. Spectroscopically confirmed stars and broad line AGNs were eliminated from the sample, leaving 6477 + 1236 galaxy spectra with secure redshift (flags 2, 3, 4, or 9), corresponding to a confidence level higher than 75%. Redshifts with flags 0 and 1 are taken into account statistically (see Sect. 4). This spectroscopic sample, which is purely magnitude selected, has a median redshift of ∼0.76.

3. Galaxy classification

Galaxies have been classified using all avaiable multicolour information; in the VVDS-02h field B, V, R and I band magnitudes are available for all galaxies, whilst U band data are available for 83% of the galaxies. For the VVDS-CDFS sample U, B, V, R and I photometry from the COMBO-17 survey is used.

Absolute magnitudes are computed following the method described in the Appendix of Ilbert et al. (2005). The K-correction is computed using a set of templates and all the photometric information (*UBVRI*) available. However, in order to reduce the template dependency, the rest frame absolute magnitude in each band is derived using the apparent magnitude from the closest observed band, shifted at the redshift of the galaxy. With this method, the applied K-correction is as small as possible.

For each galaxy the rest frame magnitudes were matched with the empirical set of SEDs described in Arnouts et al. (1999), composed of four observed spectra (CWW, Coleman et al. 1980) and two starburst SEDs computed with GISSEL (Bruzual & Charlot 1993). The match is performed minimizing a χ^2 variable on these templates at the spectroscopic redshift of each galaxy. The same procedure has been applied by Lin et al. (1999) to the CNOC-2 survey up to $z \sim 0.55$. This approach is also similar to that adopted by Wolf et al. (2003) for the COMBO-17 survey, but we have the advantage of using spectroscopic redshifts while they used photometric redshifts.

Galaxies have been divided in four types, corresponding to the E/S0 template (type 1), early spiral template (type 2), late spiral template (type 3) and irregular template (type 4). These types are based on the four CWW templates: type 4 includes also the two starburst templates. The numbers of galaxies for each type are listed in Table 1.

In order to see how these types correspond to colours, we report here the rest frame colours for each template: type 1, 2, 3 and 4 have $B_{AB} - I_{AB} = 1.58$, 1.11, 0.79 and 0.57, respectively. Given these colours, a rough colour subdivision for each class is $1.3 < B_{AB} - I_{AB}$ for type 1, $0.95 < B_{AB} - I_{AB} < 1.3$ for type 2, $0.68 < B_{AB} - I_{AB} < 0.95$ for type 3 and $B_{AB} - I_{AB} < 0.68$ for type 4. However, we emphasize that these colour ranges are indicative and our classification scheme is based on the whole multicolour coverage. In Fig. 1 we show the $U - B$ and $B - I$ colour distributions for the galaxies of our sample divided according to type. From this figure it is clear that, although the different types have different colour distributions, there are significant overlaps. This fact is a consequence of classification schemes using template fitting on multicolour data. Note that, in order to be model-independent, we did not correct our templates for colour evolution with redshift. It is well known that the colour of a passively evolving simple stellar population is bluer in the past. In principle, this could imply that galaxies classified as type 1 at low redshift might be classified differently at higher redshift. Indeed, this effect has been invoked by the authors who found negative evolution in the luminosity function of "red" galaxies (see f.i. Wolf et al. 2003). In order to test this hypothesis, we applied our classification scheme to synthetic spectra (Bruzual & Charlot 1993) of ellipticals (i.e. objects with simple stellar populations and exponentially declining star formation with time scales of 0.1 Gyr and 0.3 Gyr) with formation redshift between $z_{form} = 2$ and 20. We find that all ellipticals with $z_{form} > 2$ would be classified as type 1 objects, even at $z \sim 1$.

In order to verify, at least statistically, the consistency between this photometric classification and average spectral properties, we summed the normalised spectra of all galaxies in each of the four types. The resulting average spectra are shown in Fig. 2 for each type in various redshift bins. This figure confirms the robustness of our classification scheme: moving from type 1 to type 4 objects, the composite spectra shows an increasingly bluer continuum, with increasingly stronger emission lines. This confirms that the four types show different spectral features and therefore represent different classes of objects.

Table 1. Numbers of galaxies of different types in the sample.

Type	N_{gal}
total	7713
type 1	730
type 2	1290
type 3	2622
type 4	3071

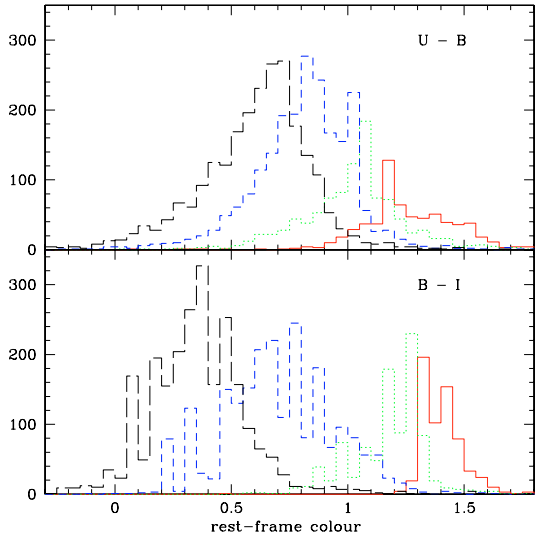

Fig. 1. Rest frame $U - B$ (*upper panel*) and $B - I$ (*lower panel*) colours for galaxies of different types: type 1 (solid line), type 2 (dotted line), type 3 (short dashed line), type 4 (long dashed line).

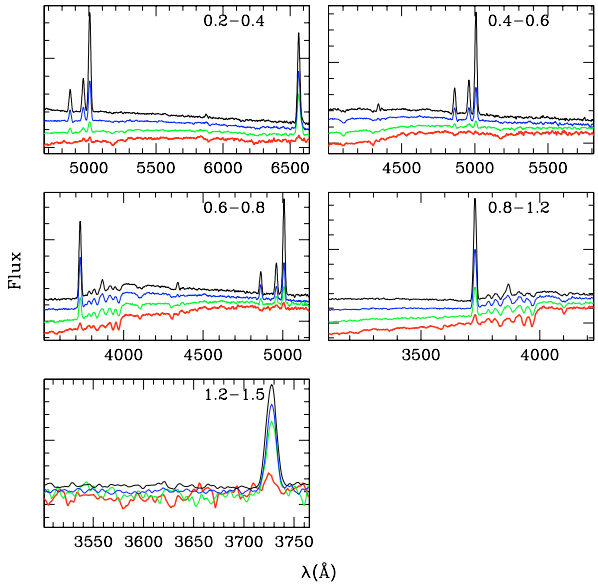

Fig. 2. Co-added VVDS spectra of galaxies of the four different types in various redshift bins, shown in rest frame wavelength. The different types are indicated with different line strengths: the lighter the line, the later the galaxy type. The redshift bin is indicated in the label of each panel. The flux on the y-axis is in arbitrary units and the spectra of the various types are arbitrarily rescaled for clarity.

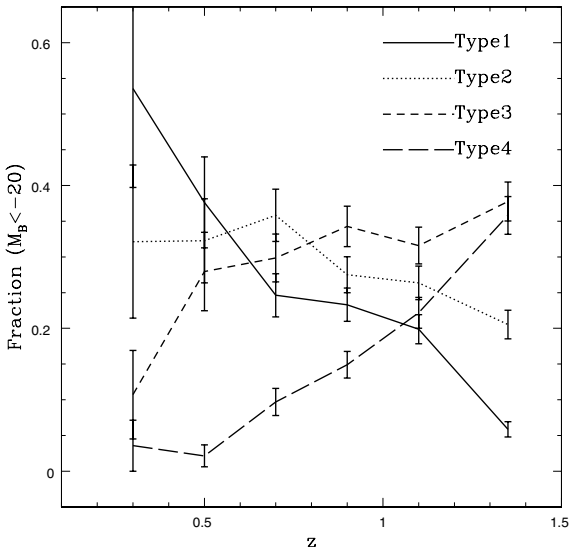

Fig. 3. Observed fraction of bright galaxies ($M_{B_{\rm AB}} - 5\log(h) < -20$) of different types as a function of redshift. Error bars are 1σ Poisson errors.

For the VVDS-CDFS sample, Hubble Space Telescope ACS images are available. Using these data, Lauger et al. (2006) classified the galaxies in this sample using an asymmetry-concentration diagram. Plotting our type 1 galaxies in this diagram, we find that ∼91% of them lie in the region of bulge dominated objects, showing an excellent consistency between our photometric and the morphological classification schemes.

In Fig. 3 we plot the observed fraction of bright galaxies of each type as a function of redshift. We selected objects with $M_{B_{\rm AB}} - 5\log(h) < -20$ as these galaxies are visible over the whole redshift range. From this figure it is clear that bright late type population becomes increasingly dominant at higher redshifts. Morever, correspondly, the fraction of bright early type galaxies decreases.

4. Computing luminosity functions

Luminosity functions were computed using the "Algorithm for Luminosity Function" (ALF), a dedicated tool which implements several estimators: the non-parametric $1/V_{\rm max}$ (Schmidt 1968), C^+ (Lynden Bell 1971), $SWML$ (Efstathiou et al. 1988) and the parametric STY (Sandage, Tammann & Yahil 1979), for which we assumed a Schechter function (Schechter 1976). The tool and these estimators, as well as their application in the context of the VVDS, are described in detail in Ilbert et al. (2005).

Ilbert et al. (2004) have shown that the estimate of the global luminosity function can be biased, mainly at the faint end, when the measurement band is far from the rest frame band in which galaxies are selected. This is due to the fact that, because of the K-corrections, different galaxy types are visible in different absolute magnitude ranges at a given redshift. When computing the global luminosity functions (Ilbert et al. 2005), we avoided this bias by using in each redshift range (for the STY estimate) only galaxies within the absolute magnitude range where all the SEDs are potentially observable.

Even if this bias is less important when estimating the luminosity function of galaxies divided by type, we have, however, taken it into account. The absolute magnitude limits for the STY estimate are indicated with vertical dashed lines in the figures, and in the tables where the best fit parameters are reported (Tables 2 and 3) we give both the total number of objects and the number of galaxies within this magnitude limit.

In order to take into account the unknown redshifts (not observed objects and failed spectra), a weight was applied to each galaxy, following the procedure described in detail in Ilbert et al. (2005).

This weight is a combination of two different contributions: the target sampling rate and the spectroscopic success rate. The target sampling rate, i.e. the fraction of observed galaxies, corrects for the selection effects due to the procedure used for the mask preparation (Bottini et al. 2005): to maximize the number of slits, the procedure tends to select objects with smaller angular size on the x-axis of the image, corresponding to the direction in which the slits are placed. As a consequence, the final spectroscopic sample has a bias against large objects, which produces a mild dependence of the target sampling rate on the apparent magnitude. The target sampling rate is ∼25% for most of the sample and is computed as a function of the object size (see Ilbert et al. 2005 for further details). The spectroscopic success rate takes into account the fraction of objects without a reliable redshift determination (i.e. flags 0 and 1). As shown in Ilbert et al. (2005), these objects are expected to have a different redshift distribution in comparison with the sample with measured redshifts (as confirmed by photometric redshifts). Given that the spectroscopic success rate decreases at fainter apparent magnitudes, we derived it for four magnitude bins as a function of redshift (using photometric redshifts, see Fig. 3 in Ilbert et al. 2005). The dependence of the spectroscopic success rate on redshift is similar in all magnitude bins, showing a maximum at $z \sim 0.7$ and two minima for $z < 0.5$ and $z > 1.5$. Since the number of galaxies for each type is not large enough to reliably estimate the spectroscopic success rate as a function also of the galaxy type, we have applied this global spectroscopic success rate to all galaxy types.

In order to check the effect of the "cosmic variance", i.e. variations in the luminosity function due to large-scale structure fluctuations, we applied the following test on the VVDS-02h deep area. For this field we derived photometric redshifts (Ilbert et al. 2006) based on both VVDS photometry

Table 2. *STY* parameters (with 1σ errors) for different galaxy types in different bands in the redshift range [0.4–0.9].

			$\Omega_m = 0.3$ $\Omega_\Lambda = 0.7$			
Band	Type	Number[a]	Number[b]	α	$M^*_{AB} - 5\log(h)$	$\phi^*\left(10^{-3}h^3\mathrm{Mpc}^{-3}\right)$
U	1	411	357	$-0.16^{+0.15}_{-0.15}$	$-19.03^{+0.14}_{-0.15}$	$3.35^{+0.20}_{-0.26}$
	2	677	596	$-0.54^{+0.12}_{-0.11}$	$-19.18^{+0.13}_{-0.14}$	$4.83^{+0.48}_{-0.53}$
	3	1371	1192	$-0.90^{+0.08}_{-0.08}$	$-19.31^{+0.11}_{-0.12}$	$7.32^{+0.86}_{-0.86}$
	4	1442	1238	$-1.66^{+0.10}_{-0.10}$	$-19.35^{+0.17}_{-0.18}$	$4.09^{+1.21}_{-1.04}$
B	1	411	404	$-0.29^{+0.10}_{-0.10}$	$-20.35^{+0.13}_{-0.13}$	$3.19^{+0.23}_{-0.26}$
	2	677	669	$-0.61^{+0.08}_{-0.08}$	$-20.25^{+0.12}_{-0.12}$	$4.48^{+0.43}_{-0.44}$
	3	1371	1349	$-0.96^{+0.06}_{-0.06}$	$-20.12^{+0.10}_{-0.11}$	$6.79^{+0.72}_{-0.71}$
	4	1442	1403	$-1.62^{+0.08}_{-0.08}$	$-19.83^{+0.15}_{-0.16}$	$4.46^{+1.08}_{-0.95}$
V	1	411	411	$-0.31^{+0.09}_{-0.09}$	$-21.13^{+0.12}_{-0.13}$	$3.16^{+0.23}_{-0.25}$
	2	677	677	$-0.61^{+0.07}_{-0.07}$	$-20.82^{+0.11}_{-0.12}$	$4.51^{+0.40}_{-0.41}$
	3	1371	1371	$-1.00^{+0.06}_{-0.06}$	$-20.57^{+0.10}_{-0.11}$	$6.21^{+0.66}_{-0.64}$
	4	1442	1442	$-1.62^{+0.08}_{-0.08}$	$-20.03^{+0.15}_{-0.16}$	$4.36^{+1.03}_{-0.92}$
R	1	411	411	$-0.31^{+0.09}_{-0.09}$	$-21.48^{+0.12}_{-0.13}$	$3.16^{+0.23}_{-0.25}$
	2	677	677	$-0.63^{+0.07}_{-0.07}$	$-21.15^{+0.11}_{-0.12}$	$4.37^{+0.40}_{-0.41}$
	3	1371	1371	$-1.05^{+0.05}_{-0.05}$	$-20.86^{+0.11}_{-0.11}$	$5.55^{+0.63}_{-0.60}$
	4	1442	1436	$-1.65^{+0.08}_{-0.08}$	$-20.18^{+0.16}_{-0.17}$	$3.87^{+0.99}_{-0.87}$
I	1	411	411	$-0.31^{+0.09}_{-0.09}$	$-21.78^{+0.12}_{-0.13}$	$3.17^{+0.23}_{-0.25}$
	2	677	677	$-0.66^{+0.07}_{-0.07}$	$-21.44^{+0.12}_{-0.12}$	$4.22^{+0.40}_{-0.40}$
	3	1371	1370	$-1.10^{+0.05}_{-0.05}$	$-21.13^{+0.11}_{-0.11}$	$5.05^{+0.60}_{-0.57}$
	4	1442	1413	$-1.67^{+0.08}_{-0.08}$	$-20.32^{+0.17}_{-0.18}$	$3.58^{+0.97}_{-0.86}$

[a] Number of galaxies in the redshift bin.
[b] Number of galaxies brighter than the bias limit (sample used for *STY* estimate; see the text for details).

Table 3. *STY* parameters (with 1σ errors) for different galaxy types in the rest frame *B* band.

				$\Omega_m = 0.3$ $\Omega_\Lambda = 0.7$		
Type	*z*-bin	Number[a]	Number[b]	α	$M^*_{AB} - 5\log(h)$	$\phi^*\left(10^{-3}h^3\mathrm{Mpc}^{-3}\right)$
					α free / α fixed	α free / α fixed
1	0.20–0.40	70	65	$-0.04^{+0.28}_{-0.27}$	$-19.81^{+0.39}_{-0.46}$ $-20.27^{+0.27}_{-0.31}$	$5.90^{+0.73}_{-0.73}$ $5.15^{+0.64}_{-0.64}$
	0.40–0.60	113	106	$-0.40^{+0.20}_{-0.20}$	$-20.71^{+0.39}_{-0.46}$ $-20.49^{+0.17}_{-0.18}$	$2.81^{+0.50}_{-0.58}$ $3.12^{+0.30}_{-0.30}$
	0.60–0.80	204	197	$-0.22^{+0.17}_{-0.17}$	$-20.14^{+0.19}_{-0.20}$ $-20.22^{+0.09}_{-0.10}$	$3.70^{+0.33}_{-0.43}$ $3.53^{+0.25}_{-0.25}$
	0.80–1.00	164	164	$-0.01^{+0.25}_{-0.24}$	$-20.46^{+0.22}_{-0.24}$ $-20.73^{+0.11}_{-0.12}$	$2.68^{+0.21}_{-0.21}$ $2.36^{+0.18}_{-0.18}$
	1.00–1.20	114	114	$-1.23^{+0.34}_{-0.34}$	$-21.49^{+0.48}_{-0.57}$ $-20.53^{+0.11}_{-0.12}$	$0.92^{+0.65}_{-0.56}$ $2.39^{+0.22}_{-0.22}$
	0.40–0.90	411	404	$-0.29^{+0.10}_{-0.10}$	$-20.35^{+0.13}_{-0.13}$	$3.19^{+0.23}_{-0.26}$
2	0.20–0.40	136	132	$-0.67^{+0.13}_{-0.13}$	$-20.29^{+0.37}_{-0.44}$ $-20.13^{+0.19}_{-0.21}$	$5.88^{+1.34}_{-1.33}$ $6.50^{+0.56}_{-0.56}$
	0.40–0.60	203	195	$-0.50^{+0.15}_{-0.14}$	$-19.81^{+0.20}_{-0.21}$ $-19.97^{+0.12}_{-0.12}$	$4.99^{+0.74}_{-0.79}$ $4.35^{+0.31}_{-0.31}$
	0.60–0.80	322	310	$-0.57^{+0.13}_{-0.13}$	$-20.33^{+0.19}_{-0.20}$ $-20.39^{+0.09}_{-0.10}$	$4.81^{+0.69}_{-0.74}$ $4.58^{+0.26}_{-0.26}$
	0.80–1.00	267	267	$-0.60^{+0.20}_{-0.20}$	$-20.54^{+0.24}_{-0.26}$ $-20.55^{+0.10}_{-0.11}$	$3.58^{+0.64}_{-0.74}$ $3.54^{+0.22}_{-0.22}$
	1.00–1.20	178	175	$-0.76^{+0.34}_{-0.33}$	$-20.92^{+0.35}_{-0.40}$ $-20.77^{+0.12}_{-0.13}$	$2.64^{+0.79}_{-0.98}$ $3.01^{+0.23}_{-0.23}$
	1.20–1.50	103	103	$-1.57^{+0.61}_{-0.62}$	$-21.65^{+0.62}_{-0.84}$ $-20.82^{+0.13}_{-0.14}$	$0.81^{+1.04}_{-0.72}$ $2.19^{+0.22}_{-0.22}$
	0.40–0.90	677	669	$-0.61^{+0.08}_{-0.08}$	$-20.25^{+0.12}_{-0.12}$	$4.48^{+0.43}_{-0.44}$
3	0.20–0.40	341	329	$-0.84^{+0.10}_{-0.10}$	$-18.92^{+0.19}_{-0.21}$ $-19.14^{+0.12}_{-0.13}$	$12.37^{+2.30}_{-2.20}$ $9.82^{+0.54}_{-0.54}$
	0.40–0.60	451	429	$-1.07^{+0.10}_{-0.10}$	$-20.28^{+0.24}_{-0.27}$ $-20.04^{+0.11}_{-0.11}$	$4.93^{+1.26}_{-1.17}$ $6.31^{+0.30}_{-0.30}$
	0.60–0.80	626	610	$-0.79^{+0.13}_{-0.13}$	$-19.86^{+0.17}_{-0.19}$ $-20.10^{+0.09}_{-0.09}$	$9.10^{+1.46}_{-1.51}$ $7.11^{+0.29}_{-0.29}$
	0.80–1.00	534	533	$-0.87^{+0.15}_{-0.15}$	$-20.23^{+0.18}_{-0.19}$ $-20.33^{+0.08}_{-0.08}$	$7.01^{+1.29}_{-1.34}$ $6.27^{+0.27}_{-0.27}$
	1.00–1.20	292	288	$-1.39^{+0.26}_{-0.26}$	$-20.82^{+0.31}_{-0.34}$ $-20.38^{+0.10}_{-0.10}$	$3.11^{+1.56}_{-1.35}$ $5.57^{+0.33}_{-0.33}$
	1.20–1.50	208	193	$-1.86^{+0.55}_{-0.59}$	$-21.87^{+0.77}_{-1.23}$ $-20.81^{+0.12}_{-0.13}$	$0.80^{+1.82}_{-0.79}$ $3.67^{+0.27}_{-0.27}$
	0.40–0.90	1371	1349	$-0.96^{+0.06}_{-0.06}$	$-20.12^{+0.10}_{-0.11}$	$6.79^{+0.72}_{-0.71}$
4	0.20–0.40	394	380	$-1.59^{+0.11}_{-0.12}$	$-19.60^{+0.46}_{-0.58}$ $-19.73^{+0.29}_{-0.33}$	$3.05^{+2.09}_{-1.67}$ $2.59^{+0.13}_{-0.13}$
	0.40–0.60	487	449	$-1.53^{+0.18}_{-0.19}$	$-19.17^{+0.33}_{-0.39}$ $-19.38^{+0.17}_{-0.18}$	$5.57^{+3.14}_{-2.56}$ $4.10^{+0.19}_{-0.19}$
	0.60–0.80	656	622	$-1.35^{+0.15}_{-0.15}$	$-19.55^{+0.20}_{-0.21}$ $-19.95^{+0.12}_{-0.12}$	$7.72^{+2.33}_{-2.09}$ $4.07^{+0.16}_{-0.16}$
	0.80–1.00	552	552	$-1.68^{+0.20}_{-0.21}$	$-20.19^{+0.31}_{-0.36}$ $-20.10^{+0.12}_{-0.12}$	$4.06^{+2.44}_{-1.93}$ $4.72^{+0.20}_{-0.20}$
	1.00–1.20	389	373	$-1.99^{+0.33}_{-0.34}$	$-20.62^{+0.41}_{-0.52}$ $-20.19^{+0.12}_{-0.12}$	$3.19^{+3.49}_{-2.22}$ $6.95^{+0.36}_{-0.36}$
	1.20–1.50	239	188	$-2.50^{+0.52}_{-0.91}$	$-21.58^{+0.76}_{-0.40}$ $-20.53^{+0.12}_{-0.12}$	$0.52^{+2.06}_{-0.29}$ $4.34^{+0.32}_{-0.32}$
	0.40–0.90	1442	1403	$-1.62^{+0.08}_{-0.08}$	$-19.83^{+0.15}_{-0.16}$	$4.46^{+1.08}_{-0.95}$

[a] Number of galaxies in the redshift bin.
[b] Number of galaxies brighter than the bias limit (sample used for *STY* estimate; see the text for details).

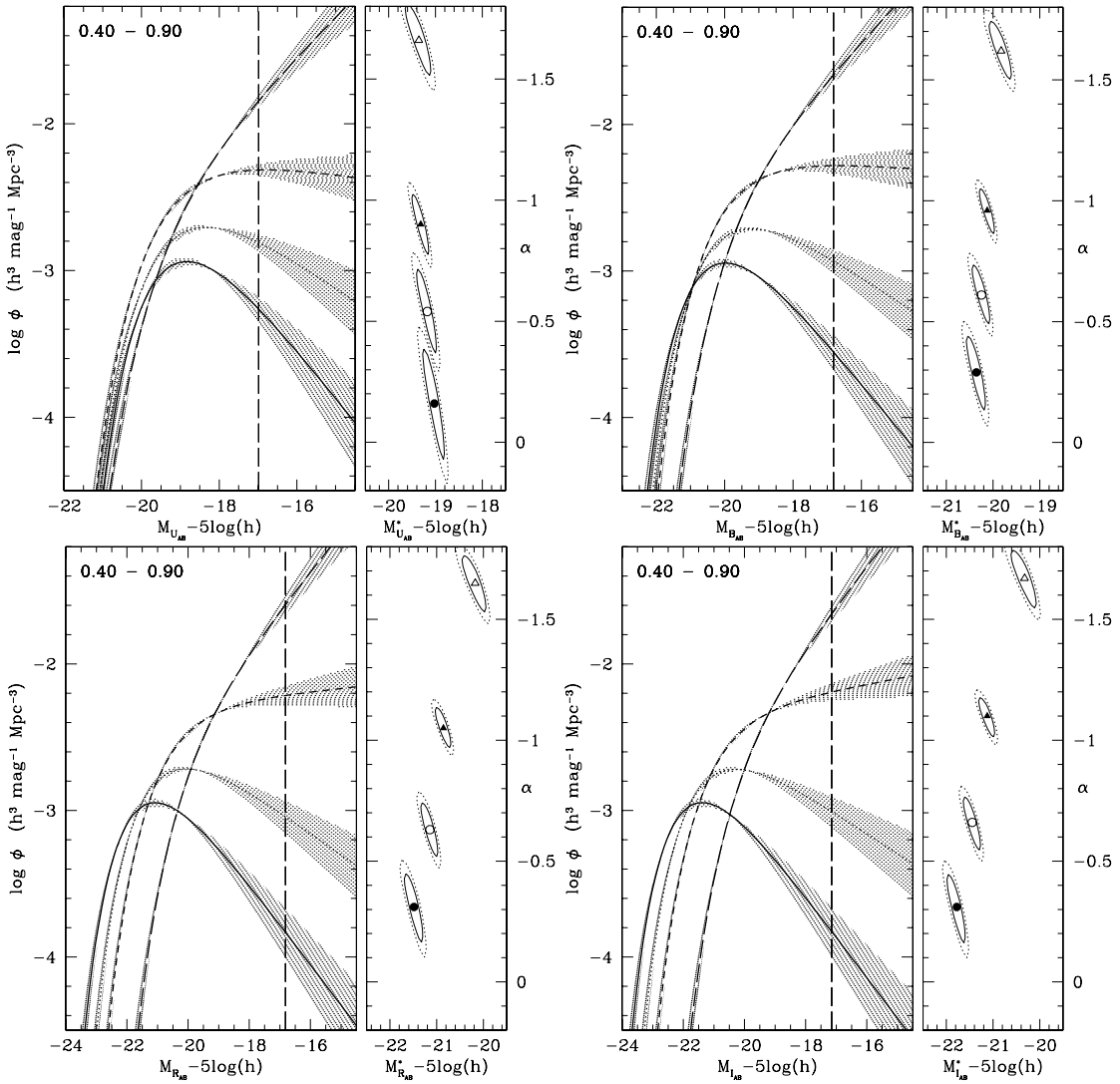

Fig. 4. Type-selected luminosity functions in the redshift range [0.4–0.9] in various rest frame bands: upper panels U (*left*) and B (*right*); *lower panels* R (*left*) and I (*right*). Note that the magnitude ranges are different in the various panels. The lines represent the STY estimates for type 1 (solid), type 2 (dotted), type 3 (short dashed) and type 4 (long dashed) galaxies. The vertical dashed line represents the faint absolute magnitude limit considered in the STY estimate (see text). The shaded regions represent the 68% uncertainties on the parameters α and M^*, whose confidence ellipses are reported in the right panels. The ellipse contours are at 68% and 90% confidence level (solid and dotted line respectively). The points inside the ellipses represent the best fit values for type 1 (filled circle), type 2 (open circle), type 3 (filled triangle) and type 4 (open triangle) galaxies.

(*BVRIJK*) and on new CFHT Legacy Survey photometry (ugriz), which is now available over a 1 sq. deg. area (`http://www.cfht.hawaii.edu/Science/CFHLS/`), including the 1750 arcmin^2 area covered by the VVDS spectroscopic survey. Then we divided the field in two non overlapping regions (the sub-area where spectroscopic data are available and the remaining area) and we compared the luminosity distributions of galaxies in these two samples (∼0.5 sq.deg. each), in the same redshift bins in which the luminosity functions were derived. In each redshift bin the two distributions show average differences of ∼10%, with some larger fluctuations due to Poisson statistics. There is no systematic trend. Therefore we expect the influence of "cosmic variance" to be limited.

5. Comparison of the type-dependent luminosity function

As a first step, we compare the luminosity functions for galaxies of different types, in order to determine the relative behaviour of the various populations. To perform this comparison, we selected galaxies in the redshift range [0.4–0.9]. About 50% of the objects in our sample are included in this redshift interval, covering a wide range of luminosities (f.i. absolute magnitudes in the B band are in the range $[-23.7; -16.8] - 5\log(h)$). Moreover, the spectroscopic success rate of our survey reaches a maximum at $z \sim 0.7$ and therefore the possible dependency of the estimated LF on the weighting scheme described above is minimized in this redshift interval.

In Fig. 4 we report the luminosity functions estimated with the STY method in the rest frame bands U, B, R and I, with the corresponding confidence ellipses for the α and M^* parameters. The values of the parameters with their 1σ errors, as well as the number of galaxies for each type, are reported in Table 2. The ϕ^* parameters listed in this table are derived adopting the density estimator of Efstathiou et al. (1988), following the procedure described in the Appendix of Ilbert et al. (2005). Table 2 shows that our estimates are based on several hundreds of galaxies for each type, and are therefore well statistically constrained

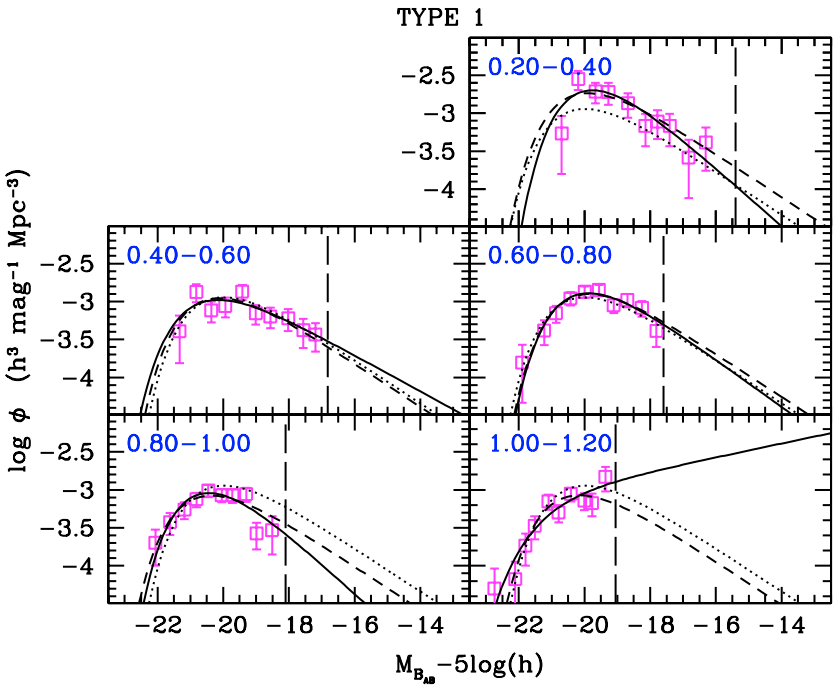

Fig. 5. Evolution of the luminosity function in the B-band for type 1 galaxies. Each panel refers to a different redshift bin, which is indicated in the label. The vertical dashed line represents the faint absolute limit considered in the STY estimate. The luminosity functions are estimated with different methods (see text for details) but for clarity we plot only the results from C^+ (open squares), and STY (solid line). The dashed line is the STY estimate obtained by fixing α to the value determined in the redshift range [0.4–0.9]. The dotted line represents the luminosity function estimated in the redshift range [0.4–0.9]: this curve is reported in each panel as a reference.

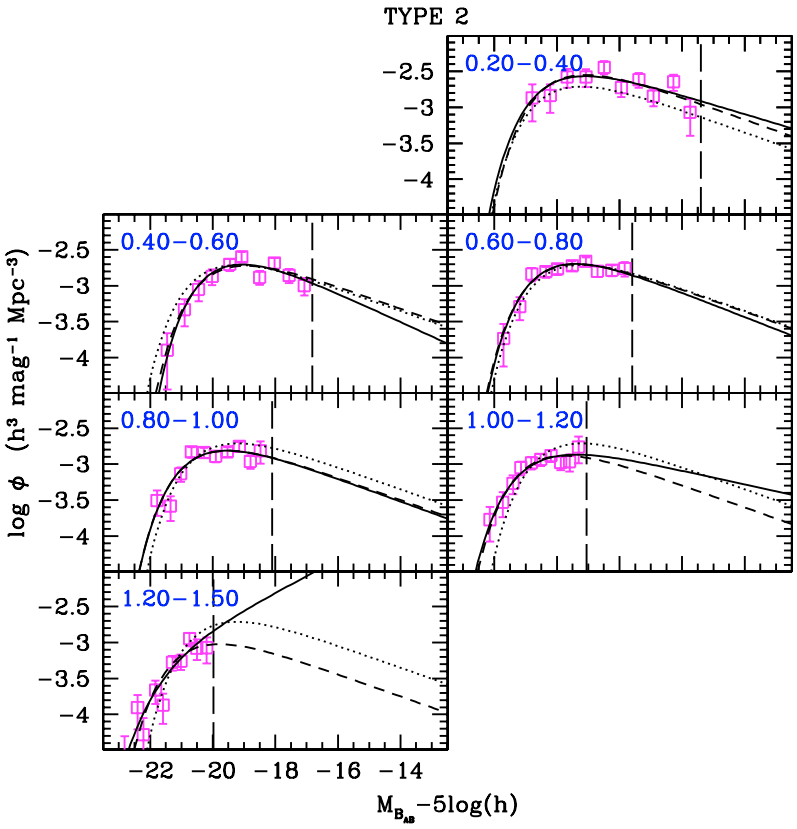

Fig. 6. Evolution of the luminosity function in the B-band for type 2 galaxies. The meaning of the lines and the symbols is the same as in Fig. 5.

as is apparent from the sizes of the confidence ellipses in the figures. The first, very clear result visible from Fig. 4 is that the luminosity functions strongly steepen from early to late types. In all bands the power law slope steepens by $\Delta\alpha \sim 1.3$–1.5 from type 1 to type 4 galaxies and galaxies of late types are the dominant population at faint magnitudes.

Systematic trends are also seen in the M^* parameter. In the reddest bands (lower panels in Fig. 4), M^* is significantly fainter for late type galaxies and this faintening is particularly apparent for type 4 objects. The brighter M^* for early type galaxies reflects the fact that most of the more massive objects belong to this population.

The difference of the M^* values between different types decreases in the B band and disappears or even changes sign in the U band. This behaviour is explained by the fact that the luminosity in the bluer bands is dominated by the light of young stars, produced during the star formation activity. Galaxies of later types, which are still actively forming stars, are therefore more luminous in the bluer bands.

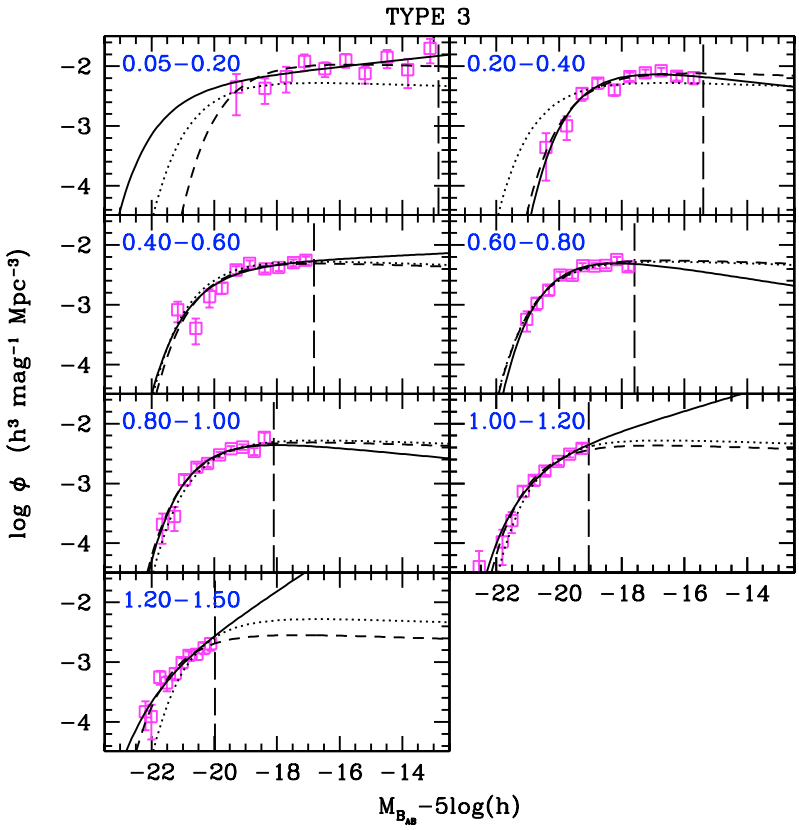

Fig. 7. Evolution of the luminosity function in the *B*-band for type 3 galaxies. The meaning of the lines and the symbols is the same as in Fig. 5.

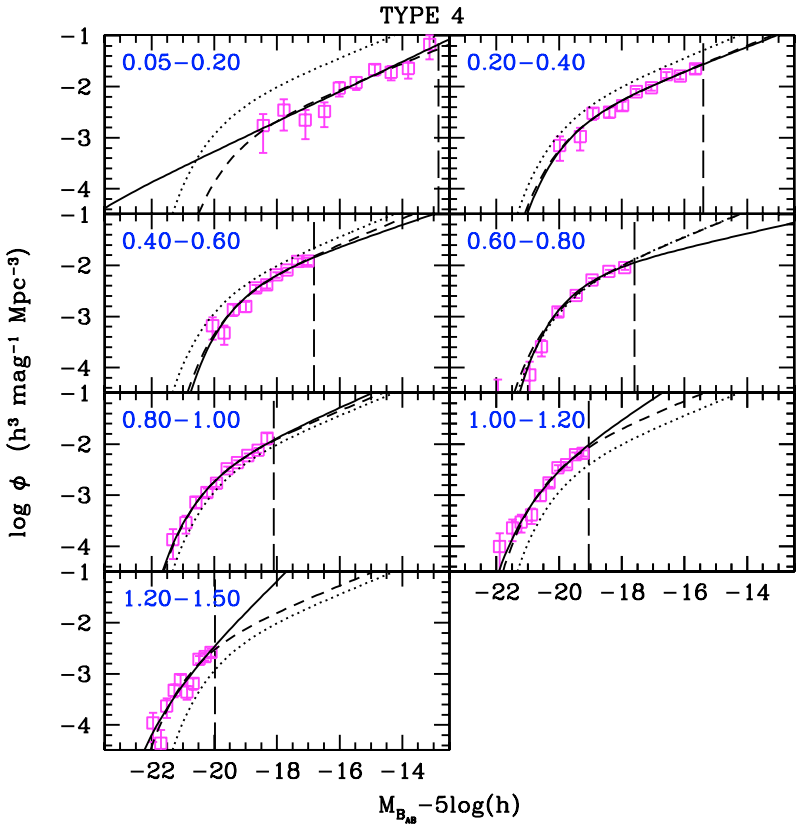

Fig. 8. Evolution of the luminosity function in the *B*-band for type 4 galaxies. The meaning of the lines and the symbols is the same as in Fig. 5.

These results are qualitatively in agreement with previous literature measurements, most of which are at lower redshifts (see de Lapparent 2003 for a review of the results from a number of surveys in the redshift range $0 \leq z \leq 0.6$). In particular, in almost all surveys the luminosity function of late type galaxies is steeper and with a fainter M^* with respect to that of early type galaxies. However, a quantitative comparison with previous results is difficult, because of their different classification scheme, redshift ranges and selection criteria.

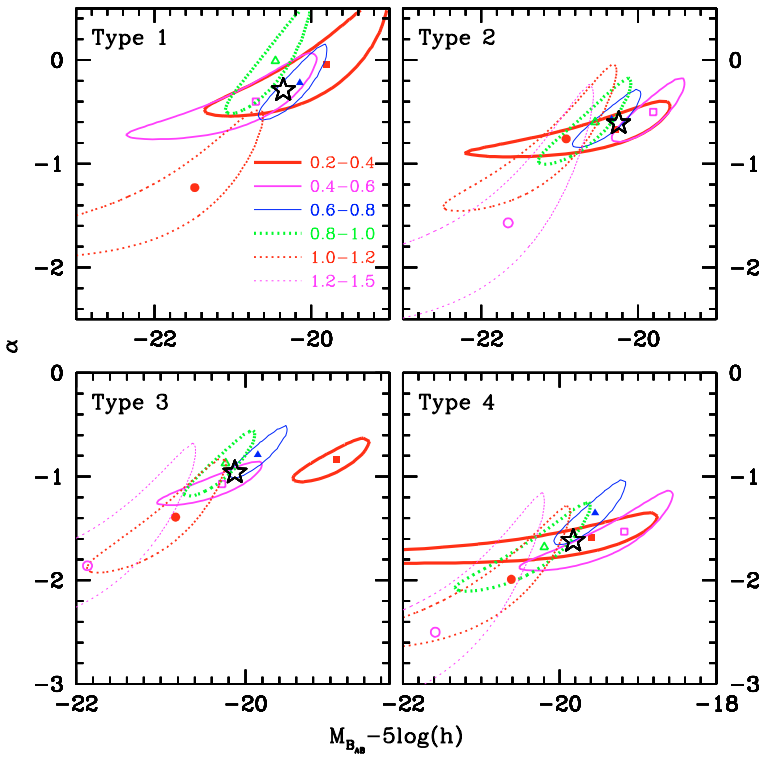

Fig. 9. 90% confidence ellipses for α and M^* luminosity function parameters reported in Figs. 5–8. Line styles and weights refer to different redshift bins, described in the labels; the points indicate the best fitting values in the redshift bins [0.2–0.4] (filled squares), [0.4–0.6] (open squares), [0.6–0.8] (filled triangles), [0.8–1.0] (open triangles), [1.0–1.2] (filled circles), [1.2–1.5] (open circles). The large open star indicates the reference value obtained in the [0.4–0.9] redshift bin.

6. Redshift evolution of the type-selected luminosity function

We derived luminosity functions for each type in redshift bins in the U, B, V, R and I rest frame bands. Given our multicolour coverage and the explored redshift range, the estimate of the absolute magnitudes in the U and B rest frame bands are those which require less extrapolations (see Appendix A and Fig. A.1 in Ilbert et al. 2005). Therefore, to limit the number of figures in the paper, we show the results in the B rest frame band.

Figures 5–8 show the luminosity function for type 1, 2, 3 and 4 galaxies in redshift bins, obtained with C^+ and STY methods. The luminosity functions derived with the other two methods ($1/V_{\rm max}$ and $SWML$) are consistent with those shown in the figures, but are not drawn for clarity. The dotted line in each panel represents the fit derived in the redshift range [0.4–0.9] (see previous section), while the dashed line is the estimate derived by fixing the slope α to the value obtained in the range [0.4–0.9].

In Table 3 we report the Schechter parameters, with their 1σ errors, estimated for various redshift bins, from $z = 0.2$ to $z = 1.5$ for each type; as a reference, in the last line we give the parameters derived in the redshift bin [0.4–0.9].

We do not show the results for bins where the number of objects is too small (less than ∼30) to constrain the parameters of the luminosity function (these are the bin [0.05–0.2] for type 1 and 2 and the bin [1.2–1.5] for type 1). For the lowest-redshift bin [0.05–0.2], the volume of the survey combined with our bright magnitude limit means we cannot sample the bright galaxy population. For this reason we are not able to determine M^* even for type 3 and 4 galaxies in this bin, where the number of objects is relatively high (∼80). For this reason we show in the figures the luminosity function estimates in this bin, but we do not report the STY parameters for this redshift range in Table 3.

In Fig. 9 we show the parameter confidence ellipses for α and M^* in different redshift bins for the different types. From this figure we can see that, within each type, the estimated slopes α in the various redshift bins are always consistent (within 90% confidence level) with each other and with the value derived in the redshift range [0.4–0.9]. Therefore, there is no evidence of a significant redshift dependency of the luminosity function slope within each galaxy type. Note also that the uncertainties on the slope estimates become quite large for $z > 1$: this is due to the fact that, even with the faint limit ($I_{\rm AB} \leq 24$) of this survey, the number of galaxies fainter than M^* is too low to constrain the slope.

In each panel of Figs. 5–8 we draw, as a reference, the luminosity function derived in the redshift bin [0.4–0.9] (dotted line). Comparing this curve with the estimates of the luminosity function at each redshift bin evolutionary effects are evident which depend strongly on galaxy type. This evolution is particularly evident for type 4 galaxies: going from low to high redshift there is an almost continuous brightening of M^* and at fixed luminosity the density of these galaxies was much higher in the past.

The observed evolution of the luminosity function could be due to an evolution in luminosity and/or in density or both. One of the advantages of the STY method is that it allows one to derive α and M^* parameters independently from ϕ^*, which is not possible when one directly fits a Schechter function to the $1/V_{\rm max}$ points.

Given the fact that we found that α is consistent with being type-independent, we can fix it at the reference value derived in the redshift range [0.4–0.9] and then study the variations of the parameters M^* and ϕ^* as a function of redshift (see upper and middle panels of Fig. 10). These estimates are reported in Table 3.

From Fig. 10 we can see a mild evolution of M^* from the lowest to the highest redshift bin for each type. In particular, this brightening ranges from $\lesssim$0.5 mag for early type galaxies to ∼1 mag for the latest type galaxies. The only exception with respect to the general trend is that of type 3 objects in the bin [0.2–0.4], for which the best fit value of the M^* parameter is significantly fainter than expected. The reason for this discontinuity in M^* for type 3 galaxies at low redshift is not clear.

On the contrary, the ϕ^* parameter shows a very different behaviour for type 1, 2 and 3 galaxies with respect to type 4 galaxies. The first three types show a rapid decrease of ϕ^* at low redshifts (between $z \sim 0.3$ and $z \sim 0.5$), then ϕ^* remains roughly constant up to $z \sim 0.9$ and finally slowly decreases up to $z = 1.5$.

Type 4 objects, on the contrary, show an increase in ϕ^* at low redshift, then ϕ^* is nearly constant up to $z \sim 0.8$ and shows a rapid increase of a factor ∼2 at $z = 1.1$. Then there seems to be a decrease from $z = 1.1$ to $z = 1.3$. However, this is mostly likely a spurious effect, due to the fact that in this bin the estimated M^* is very close to the bias limit (see Sect. 4). If, for example, we fix M^* to the value obtained in the previous redshift bin $[1.0 - 1.2]$, we derive a significantly higher value for ϕ^*, i.e. $\phi^* = 5.83 \times 10^{-3} h^3 \mathrm{Mpc}^{-3}$ (corresponding to $\phi^*/\phi^*_{\mathrm{ref}} = 1.31$). Therefore the last ϕ^* value for type 4 galaxies is likely to be a lower limit of the true density value.

This analysis of the redshift dependence of ϕ^* indicates that the importance of type 4 galaxies increases with redshift. However, since M^* also changes with redshift (see above), the behaviour of ϕ^* can not be immediately interpreted in terms of density at a given absolute magnitude. For this reason, we have computed the density of bright galaxies as a function of redshift. We integrated the best fit luminosity function down to $M_{B_{\mathrm{AB}}} - 5\log(h) < -20$. This limit approximately corresponds to the faintest galaxies which are visible over the entire redshift range. In the lowest panel of Fig. 10 we plot the density of bright galaxies of each type as a function of redshift.

The main results shown in this plot can be summarised as follows:

a. the density of bright early type galaxies (type 1) decreases with increasing redshift. However this decrease is rather modest and is around ∼40% from $z \sim 0.3$ to $z \sim 1.1$;
b. conversely, the density of bright late type galaxies (type 4) increases significantly, by a factor ∼6.6 from $z \sim 0.3$ to $z \sim 1.3$.

It is the type 4 galaxies which are also responsible of the evolution of the global luminosity function measured by Ilbert et al. (2005). In fact, the increasing number of both faint and bright type 4 galaxies leads to the steepening of the global LF (due to the very steep slope of type 4 LF) and to the brightening of M^* (due to the increasing fraction of bright blue objects). This fact has been directly checked summing the LF of all types and comparing the result with the global LF estimate.

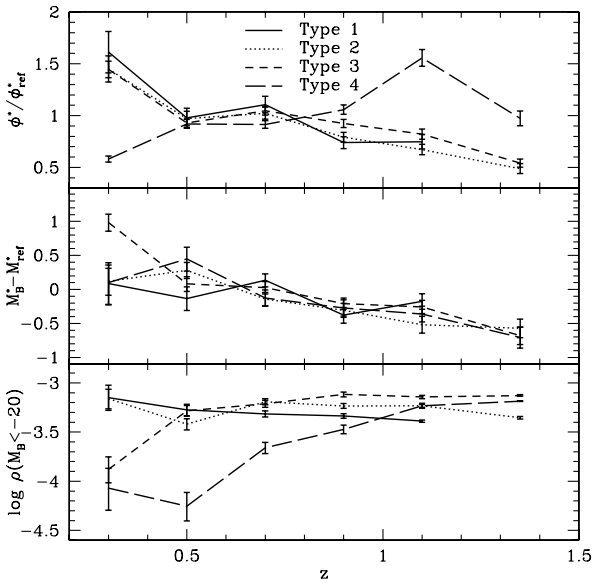

Fig. 10. Evolution of the parameters ϕ^* (*upper panel*) and M^* (*middle panel*) as a function of the redshift, for different galaxy types. In the lowest panel the density of bright ($M_{B_{\mathrm{AB}}} - 5\log(h) < -20$) galaxies of different types is shown. The slope α is fixed to the value derived in the redshift range [0.4–0.9]; the suffix "ref" indicates the parameters estimated in the redshift range [0.4–0.9]. Error bars are at 1σ.

7. Comparison with previous literature results

Although several estimates of the luminosity function by galaxy type have been published, quantitative comparisons of our results with previous analyses is problematic. This is because each survey, in general, adopts different classification schemes, different numbers of galaxy types, which are investigated over different redshift ranges and using different selection criteria.

The strong density evolution of late type galaxies we find in the redshift range [0.2–1.5] extends to significantly higher redshift the results found by de Lapparent et al. (2004) for their latest type at $z \sim 0.5$.

Amongst the other surveys CNOC-2 (Lin et al. 1999) and COMBO-17 (Wolf et al. 2003) adopted a classification scheme approximately similar to ours. Lin et al. (1999) divided their sample of galaxies with $z < 0.55$ in three classes (early, intermediate and late type) using CWW templates. For early type galaxies they found a positive luminosity evolution, which is almost compensated by a negative density evolution. On the contrary, for late type galaxies they found a strong positive density evolution, with nearly no luminosity evolution. We see at higher redshift the same trend in density, but our evolution in M^* is limited to within one magnitude for each type. Wolf et al. (2003) used a sample of ∼25 000 galaxies with photometric redshifts, applying a classification scheme in four classes similar to ours but using the Kinney et al. (1996) templates instead of the CWW templates.

In Fig. 11 we compare our results (solid lines) with those from COMBO-17 (dashed lines). Note that, since our data extend always to fainter absolute magnitudes, in particular for type 1 galaxies, our estimates of the faint end slope are likely to be more reliable: these estimates are derived in each redshift bin, while the COMBO-17 slopes are fixed to the value determined in the redshift range [0.2–0.4]. This figure shows that there are significant differences in both shapes and evolution of the LF estimates. The slope of the COMBO-17 LF is flatter than ours for type 1 galaxies, while it is steeper for types 2 and 3 (at least up to $z = 1.0$). The most significant difference between the two surveys concerns the evolution of type 1 galaxies, for which we do not have any evidence of the very strong density decrease with increasing redshift found in the COMBO-17 sample. The reason for this difference is unclear: it could be due to the use of different templates in the definition of the galaxy types or to a degeneracy between photometric redshift and classification, which might affect the COMBO-17 data. Bell et al. (2004) explained the strong negative evolution of type 1 galaxies as a consequence of the blueing with increasing redshift of elliptical galaxies with respect to the classification template. In this way, at higher redshifts an increasing number of "ellipticals" would be assigned to later types, therefore producing the density decrease observed in COMBO-17 data. However, as mentioned in Sect. 3, we verified that this effect does not affect our classification scheme, at least up to $z \sim 1$ and for simple stellar populations with $z_{\mathrm{form}} > 2$.

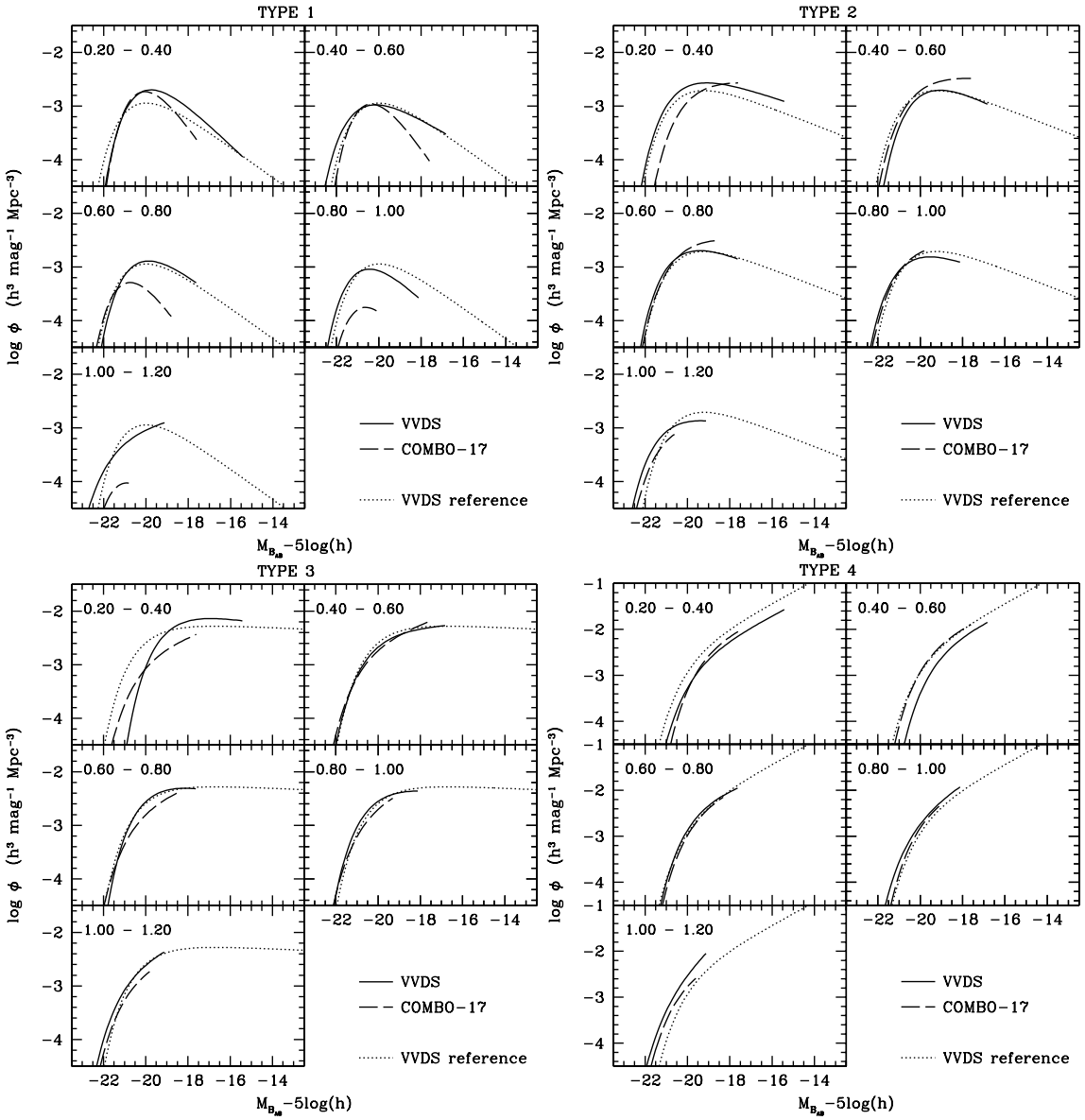

Fig. 11. Comparison between VVDS and COMBO-17 luminosity functions, in various redshift bins (indicated in the label in each panel) and for various types. *Upper panels*: type 1 (*left*) and type 2 (*right*) galaxies. *Lower panels*: type 3 (*left*) and type 4 (*right*) galaxies. Solid lines: VVDS estimate. Dotted lines: VVDS estimate in the redshift range [0.4–0.9], plotted as a reference. Dashed line: COMBO-17 estimate from Wolf et al. (2003).

As a test of this possible effect, we compared the LF obtained by adding together type 1 and 2 objects. In this way we can check whether the differences between VVDS and COMBO-17 LF of type 1 galaxies is because a significant fraction of high redshift type 1 galaxies in COMBO-17 are classified as type 2 galaxies. This comparison is shown in Fig. 12. The discrepancy between VVDS and COMBO-17 LF is now smaller, but there are still significant differences both in slope (the COMBO-17 LF is steeper than that of VVDS) and in normalization, especially in the highest redshift bin, where the VVDS LF is more than a factor of two higher than the COMBO-17 LF.

8. Conclusions

In this paper we studied the evolution of the luminosity function of different galaxy types up to $z = 1.5$, using 7713 spectra with $17.5 \leq I_{\rm AB} \leq 24$ from the first epoch VVDS deep sample.

With the VVDS data we can for the first time study with excellent accuracy the evolution of the type-dependent luminosity functions from relatively low redshifts up to $z = 1.5$ within the same purely magnitude selected spectroscopic sample. The faint limiting magnitude of the VVDS sample allows measurement of the faint-end slope of the luminosity function with unprecedented accuracy out to $z \sim 1.2$. Spectroscopic redshifts ensure a much lower contamination by "catastrophic" failures compared to the photometric redshifts and for this reason rare populations (such as the bright galaxies) are much better sampled. Moreover, the use of spectroscopic redshifts allows a galaxy classification which avoids degeneracies between photometric redshift and classification.

VVDS galaxies were classified in four spectral classes using their colours and redshift, from early type to irregular galaxies, and luminosity functions were derived for each type in redshift bins, from $z = 0.05$ to $z = 1.5$, in the U, B, V, R and I rest frame bands.

We find the slope of the luminosity function steepens strongly from early to late types: in all bands the power law slope steepens by $\Delta\alpha \sim 1.3$–1.5 from type 1 to type 4. Moreover, the

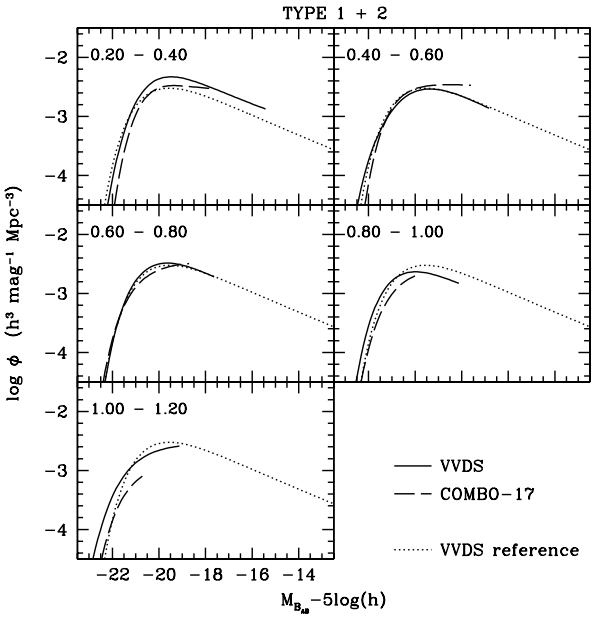

Fig. 12. Comparison between VVDS and COMBO-17 luminosity functions, in various redshift bins (indicated in the label in each panel) for the sum of types 1 and 2. The meaning of the symbols is the same as in Fig. 11.

M^* parameter of the Schechter function is significantly fainter for late type galaxies. As expected, this difference increases in the redder bands, reaching ∼1.4 mag in the I band. Investigating the variations with redshift of the luminosity function for each type, we find that there is no evidence of a significant change of the slope. However we find a brightening of M^* with increasing redshift, ranging from $\lesssim$0.5 mag for early type galaxies to ∼1 mag for the latest type galaxies. We also find a strong evolution in the normalisation of the luminosity function of latest type galaxies, with an increase of more than a factor 2 in the ϕ^* parameter going from $z \sim 0.3$ to $z \sim 1.3$. The density of bright ($M_{B_{\rm AB}} - 5\log(h) < -20$) galaxies shows a modest decrease (∼40%) for early type objects from $z \sim 0.3$ to $z \sim 1.1$; on the contrary, the number of bright late type galaxies increases of a factor ∼6.6 from $z \sim 0.3$ to $z \sim 1.3$.

Our results indicate that the importance of type 4 galaxies increases with redshift, with an important contribution coming from both bright and faint blue objects. This fact is also largely responsible of the evolution of the global luminosity function measured by Ilbert et al. (2005), which shows a brightening of M^* and a steepening of α with increasing redshift. Moreover, the increasing contribution of blue galaxies has been also seen in the evolution of the GALEX-VVDS luminosity function at 1500 Å (Arnouts et al. 2005). We are therefore identifiying that the galaxies responsible for most of the evolution quoted in the literature belong to the population of the latest spectral type. The epoch at which a transition between a Universe dominated by late type galaxies and a Universe dominated by old massive objects occurs is at a redshift of z ∼0.7–0.8.

The fact that type 1 galaxies show only a mild evolution both in luminosity (positive) and in density (negative) is consistent with the observation that most of the objects in this class are old ($z_{\rm form} > 2$, see Sect. 3) galaxies, experiencing only a passive evolution in the explored redshift range. More intriguing is the density evolution of type 4 galaxies, which corresponds to an increasing number of bright star forming galaxies at higher redshifts which could be connected to various populations of high redshift objects seen in multiwavelength surveys.

Acknowledgements. This research has been developed within the framework of the VVDS consortium. This work has been partially supported by the CNRS-INSU and its Programme National de Cosmologie (France), and by Italian Ministry (MIUR) grants COFIN2000 (MM02037133) and COFIN2003 (num.2003020150).

The VIMOS VLT observations have been carried out on guaranteed time (GTO) allocated by the European Southern Observatory (ESO) to the VIRMOS consortium, under a contractual agreement between the Centre National de la Recherche Scientifique of France, heading a consortium of French and Italian institutes, and ESO, to design, manufacture and test the VIMOS instrument.

References

Arnouts, S., Cristiani, S., Moscardini, L., et al. 1999, MNRAS, 310, 540
Arnouts, S., Vandame, B., Benoist, C., et al. 2001, A&A, 379, 740
Arnouts, S., Schiminovich, D., Ilbert, O., et al. 2005, ApJ, 619, L43
Bell, E. F., Wolf, C., Meisenheimer, K. et al. 2004, ApJ, 608, 752
Blanton, M. R., Dalcanton, J., Eisenstein, D., et al. 2001, AJ, 121, 2358
Blanton, M. R., Hogg, D. W., Bahcall, N. A., et al. 2003, ApJ, 592, 819
Bondi, M., Ciliegi, P., Zamorani, G., et al. 2003, A&A, 403, 857
Bottini, D., Garilli, B., Maccagni, D., et al. 2005, PASP, 117, 996
Bruzual, G., Charlot, S. 1993, ApJ, 405, 538
Caputi, K. I., McLure, R. J., Dunlop, J. S., Cirasuolo, M., Schael, A. M. 2006, MNRAS, 366, 609
Ciliegi, P., Zamorani, G., Bondi, M., et al. 2005, A&A, 441, 879
Cimatti, A., Mignoli, M., Daddi, E., et al. 2002, A&A, 392, 395
Coleman, G. D., Wu, C. C., & Weedman, D. W. 1980, ApJS, 43, 393
Dahlen, T., Mobasher, B., Somerville, R., et al. 2005, ApJ, 631, 126
Davis, M., Faber, S. M., Newman, J., et al. 2003, SPIE, 4834, 161
de Lapparent, V. 2003, A&A, 408, 845
de Lapparent, V., Galaz, G., Bardelli, & S., Arnouts, S. 2003, A&A, 404, 831
de Lapparent, V., Arnouts, S., Galaz, G., & Bardelli, S. 2004, A&A, 422, 841
Efstathiou, G., Ellis, R. S., Peterson, B.A. 1988, MNRAS, 232, 431
Faber, S. M., Willmer, C. N. A., Wolf, C., et al. 2006, ApJ, submitted [arXiv:astro-ph/0506044]
Gabasch, A., Bender, R., Seitz, S., et al. 2004, A&A, 421, 41
Giallongo, E., Salimbeni, S., Menci, N., et al. 2005, ApJ, 622, 116
Ilbert, O., Tresse, L., Arnouts, S., et al. 2004, MNRAS, 351, 541
Ilbert, O., Tresse, L., Zucca, E., et al. 2005, A&A, 439, 863
Ilbert, O., Arnouts, S., McCracken, H.J., et al. 2006, A&A, accepted [arXiv:astro-ph/0603217]
Iovino, A., McCracken, H. J., Garilli, B., et al. 2005, A&A, 442, 423
Kinney, A. L., Calzetti, D., Bohlin, R. C., et al. 1996, ApJ, 467, 38
Lauger, S., Ilbert, O., Burgarella, D., et al. 2006, A&A, in press
Le Fèvre, O., Vettolani, G., Maccagni, D., et al. 2003a, SPIE, 4841, 1670
Le Fèvre, O., et al. 2003b, proc. of IAU Symp. 216, Maps of the Cosmos, Sydney, July 2003, ed. M. Colless & L. Staveley-Smith, in press [arXiv:astro-ph/0311475]
Le Fèvre, O., Mellier, Y., McCracken, H. J., et al. 2004a, A&A, 417, 839
Le Fèvre, O., Vettolani, G., Paltani, S., et al. 2004b, A&A, 428, 1043
Le Fèvre, O., Vettolani, G., Garilli, B., et al. 2005a, A&A, 439, 845
Le Fèvre, O., Guzzo, L., Meneux, B., et al. 2005b, A&A, 439, 877
Lilly, S. J., Tresse, L., Hammer, F., Crampton, & D., Le Fèvre, O. 1995, ApJ, 455, 108
Lin, H., Yee, H. K. C., Carlberg, R. G., et al. 1999, ApJ, 518, 533
Lynden Bell, D. 1971, MNRAS, 155, 95
Madgwick, D., Lahav, O., Baldry, I. K., et al. 2002, MNRAS, 333, 133
Marinoni, C., Le Fèvre, O., Meneux, B., et al. 2005, A&A, 442, 801
McCracken, H. J., Radovich, M., Bertin, E., et al. 2003, A&A, 410, 17
Norberg, P., Cole, S., Baugh, C. M., et al. 2002, MNRAS, 336, 907
Poli, F., Menci, N., Giallongo, E., et al. 2001, ApJ, 551, L45
Poli, F., Giallongo, E., Fontana, A., et al. 2003, ApJ, 593, L1
Pollo, A., Meneux, B., Guzzo, L., et al. 2005, A&A, 439, 887
Pozzetti, L., Cimatti, A., Zamorani, G., et al. 2003, A&A, 402, 837
Radovich, M., Arnaboldi, M., Ripepi, V., et al. 2004, A&A, 417, 51
Sandage, A., Tammann, G. A., & Yahil, A. 1979, ApJ, 232, 352
Saracco, P., Fiano, A., Chincarini, G., et al. 2006, MNRAS, 367, 349
Sawicki, M. J., Lin, H., & Yee, H. K. C. 1997, AJ, 113, 1
Scaramella, R., et al. 2006, in preparation
Schechter, P. 1976, ApJ, 203, 297
Schiminovich, D., Ilbert, O., Arnouts, S., et al. 2005, ApJ, 619, L47
Schmidt, M. 1968, ApJ, 151, 393
Scodeggio, M., Franzetti, P., Garilli, B., et al. 2005, PASP, 117, 1284
Tresse, L., et al. 2006, A&A, submitted
Wolf, C., Meisenheimer, K., Rix, H.W., et al. 2003, A&A, 401, 73
Zanichelli, A., Garilli, B., Scodeggio, M., et al. 2005, PASP, 117, 1271